Available online at www.sciencedirect.com
SCIENCE DIRECT
Journal of Catalysis 229 (2005) 389–403
JOURNAL OF CATALYSIS
www.elsevier.com/locate/jcat

Influence of pH on noble metal catalysed alcohol oxidation: reaction kinetics and modelling

V.R. Gangwal, J. van der Schaaf, B.F.M. Kuster, J.C. Schouten *

Laboratory of Chemical Reactor Engineering, Department of Chemical Engineering & Chemistry, Eindhoven University of Technology, P.O. Box 513, 5600 MB Eindhoven, The Netherlands

Received 7 October 2004; revised 11 November 2004; accepted 12 November 2004

Available online 23 December 2004

Abstract

The Pt-catalysed oxidation of the alcohol methyl α-D-glucopyranoside to 1-O-methyl α-D-glucuronic acid has been studied under varying pH conditions. Two types of catalysts with different metal dispersion are used, that is, Pt on active carbon support and Pt on graphite support. The pH of the reaction medium is varied between 6 and 10. The initial reaction rate increases with an increase in pH, and so does the rate of catalyst deactivation, because of overoxidation, for both catalysts. The carbon-supported Pt catalyst gives higher initial reaction rates compared with the graphite-supported Pt catalyst.

A dynamic, pH-dependent, electrochemical kinetic model is presented based on a detailed investigation of the mechanism of alcohol oxidation. The model adequately describes the observed pH effect by considering the alcohol dehydrogenation occurring in two parallel reaction steps, one playing a role under acidic conditions, which is independent of the hydroxyl concentration, and a second one playing a role under alkaline conditions, which is linearly dependent on the hydroxyl concentration.

Keywords: pH Effect; Electrochemical kinetic model; Alcohol oxidation; Pt catalyst; Parameter estimation; Modelling; Catalyst deactivation; Reactivation

1. Introduction

Traditionally, because of fast production demands and one-pot operation, synthesis routes of fine chemical and pharmaceutical compounds have been based on alcohol oxidation with stoichiometric quantities of inorganic oxidants. This oxidation process suffers from low atom efficiency and high toxic waste production [1]. Alcohol oxidation by enzymes is practiced as an environmentally friendlier alternative; however, product separation and waste production remain a problem. Homogeneous catalysis is an efficient alternative; however, catalyst recovery, reactant recycling, and reactor corrosion limit its utilisation on an industrial scale. A recent review of Mallat and Baiker [2] gives an extensive survey of "green" methods for heterogeneously catalysed alcohol oxidation. Noble metal-catalysed alcohol oxidation with cheap oxidants such as air or molecular oxygen is a clean and elegant alternative with mild reaction conditions, with which high selectivities can be obtained [3–5].

Generally, aqueous alcohol oxidation is carried out in a weakly acidic or alkaline medium (pH 6–11). The influence of pH on alcohol oxidation is complex and difficult to study, as the pH can influence the reaction in several direct and indirect ways [4]. Multiple influences of pH have been reported. First, with an increase in pH, the rate of oxidation increases in an alkaline medium [6–9]. Second, the selectivity towards the aldehyde intermediate decreases with increasing pH [10,11]. Third, at low pH (< 6), product adsorption to the catalyst strongly inhibits the reaction [12]. Finally, at high pH (> 11), the formation of by-products or leaching of the catalyst inhibits the reaction [13,14]. However, in the case of alcohols with low acidity (high pK_a value) and strong reducing ability, the pH has no influence on the oxidation rate [14–16]. Vleeming et al. showed that with Pt on graphite catalyst, the rate of initial oxidation decreases with an in-

* Corresponding author. Fax: +31-40-2446653.
E-mail address: j.c.schouten@tue.nl (J.C. Schouten).

0021-9517/$ – see front matter
doi:10.1016/j.jcat.2004.11.021

crease in pH from 8 to 10 [11]. However, in an earlier study with Pt on carbon catalyst, a linear increase of the rate at pH > 8.5 was reported [8]. These seemingly contradictory findings may be due to the multiple influences of pH, on the interaction of the catalyst support with adsorbed reactant alcohol and/or oxygen species, the concentration of intermediate aldehyde and (side) products, and catalyst deactivation due to overoxidation.

Several types of catalyst deactivation mechanisms have been identified, such as overoxidation (corrosion), decarbonylation (CO formation), aldol condensation (polymerisation or coking), crystalline growth (Ostwald ripening), and metal dissolution (leaching) [17]. These deactivation mechanisms lead to a decrease in the active metal surface area and hence to a decrease in the reaction rate.

In electrochemistry research, reactions are carried out without oxidising agents like oxygen but with electrode potentials. At low potential (< 0.4 V RHE) in acidic or neutral medium, CO poisoning is the main cause of catalyst deactivation [18,19]. However, most of the experimental evidence on CO poisoning is obtained from methanol oxidation experiments [20,21]. The formation of adsorbed CO can be reduced or avoided with an increase in the pH of the solution or by promoting electrode potential (> 0.7 V RHE) or with electrodes of heavy metals, such as Bi, Pb, etc. [20,22].

In gas–solid catalysis, extensive work has been done on the decomposition pathways of alcohols and aldehydes on single crystal metal surfaces [23]. A fundamental surface science study on a Pd metal surface under ultrahigh vacuum (UHV) conditions has demonstrated that on a clean or oxygen-free Pd surface, decarbonylation is inevitable, whereas oxygen-covered surfaces suppress decarbonylation reactions [24].

There is hardly any evidence of CO formation under normal conditions of liquid-phase heterogeneous alcohol oxidation. CO formation has been observed only under oxygen mass transport limited conditions, for certain compounds like aromatic alcohols and aldehydes [25]. In the absence of oxygen mass transport limitations, the study of Abbadi et al. on the influence of pH on Pt-catalysed D-glucose oxidation revealed that the "free" form of the product, D-gluconic acid, and not CO is the main poisoning species in an acidic medium [12]. In weakly alkaline or acidic medium under kinetic limited conditions, overoxidation has been observed to be the main cause of catalyst deactivation [26–29].

The present work focuses on the Pt-catalysed oxidation of a primary polyol under oxygen-rich conditions (> 0.7 V RHE), in which CO formation or deposition of carbonaceous species is unlikely [30]. Furthermore, for the investigated pH range, it is unlikely that the aldol reaction would result in a high-molecular-weight by-product [8,28]. Hence, these types of catalyst deactivation are excluded from the present kinetic model. In addition, long-term catalyst deactivation by coking, attrition, crystalline growth, and leaching is not subject of this study, and care has been taken to avoid these types of deactivation. It was verified through intermediate catalyst reactivation that overoxidation was the main cause of the catalyst deactivation.

In the literature some efforts have been made to model the possible effects of pH on alcohol oxidation. Schuurman et al. performed initial rate kinetic modelling by considering two reaction paths; the first involved adsorbed alcohol dominating at low pH, and the second involved alcohol anion dominating at high pH [8]. In previous work, another approach was shown in electrochemical kinetic modelling through oxygen and oxide reduction, which are proton concentration-dependent steps [31,32]. However, these models are inadequate for describing the effects of pH associated with catalyst deactivation due to overoxidation.

The goal of this work is to develop a dynamic electrochemical kinetic model that quantitatively describes the observed reaction rates and the catalyst deactivation due to overoxidation. In addition, the model provides a better understanding of the effect of catalyst support and active metal dispersion in relation to catalyst deactivation. Experiments are performed at pH values between 6 and 10, with carbon- and graphite-supported Pt catalyst, for methyl α-D-glucopyranoside (MGP) oxidation as a test reaction.

2. Mechanistic steps of alcohol oxidation

It is generally accepted, in both heterogeneous catalysis and electrochemistry, that liquid-phase alcohol oxidation on noble metal catalysts takes place via a dehydrogenation mechanism followed by the oxidation of the adsorbed hydrogen atom with dissociatively adsorbed oxygen [5–7,15,33–36]. Alternative mechanisms, such as direct involvement of the oxidising species in the rate-determining step of dehydrogenation [8,16,17,26,37,38] and, more recently, oxygen-assisted dehydrogenation mechanisms [25] have also been proposed. However, the exact reaction sequence through which the dehydrogenation mechanism occurs is still under dispute [39], because of the complex nature of the adsorbed species on the metal surface, such as the origin of adsorbed oxygen species, O_2 or OH^- or H_2O, or the type of adsorbed reactant alcohol, RCH_2OH or RCH_2O^- or RCH_2O. The nature of the adsorbed species mainly depends on the pH of the reaction medium, the concentration of the oxidising agent, and the acidity of the catalyst.

Several possible reaction sequences describing the global reaction of alcohol oxidation with oxygen on Pt catalysts by different adsorption and surface reaction steps have been considered in the literature. Excluding formation of CO and carbonaceous deposits, three steps (in any order) can be identified as important ones:

1. Oxygen adsorption and reduction.
2. Alcohol/aldehyde dehydrogenation.
3. Platinum oxide formation that is, overoxidation or corrosion (deactivation) and reduction (reactivation).

2.1. Oxygen adsorption and reduction

One of the most essential functions of the catalyst is the activation of oxygen. The way in which oxygen becomes activated is a crucial problem in oxidation catalysis [40]. Generally speaking, oxygen activation is assumed to occur by its adsorption. Oxygen may adsorb to metal surfaces as

1. Weakly adsorbed molecular oxygen.
2. Chemisorbed atomic oxygen.
3. Oxygen atoms penetrating the most external layers of metal crystals, thus forming "subsurface" oxygen.

The kind of metal oxygen bond depends on the purity of the metal surfaces, temperature, and the crystal face being studied. At platinum (111), molecular adsorption of oxygen is predominant below 120 K and exhibits a desorption peak at 150 K,

$$O_2 + * \rightleftharpoons O_2*, \quad (1)$$

$$O_2 + e^- + * \rightleftharpoons O_2{}^-*, \quad (2)$$

where $*$ is the free adsorption site.

In the case of silica-supported and presumably finely divided platinum, $O_2{}^-$ species were identified by electron spin resonance (EPR) measurements at ambient temperature; O^- species were also present [40]. Electron transfer from the metal to oxygen results in a positive potential of the metal, up to 1.5 V RHE [41]. Molecularly adsorbed oxygen plays the role of precursor to adsorbed atomic oxygen:

$$O_2* + * \rightleftharpoons 2O*, \quad (3)$$

$$O_2{}^-* + e^- + * \rightleftharpoons 2O^-*. \quad (4)$$

Atomic oxygen at the surface of Pt is the predominant form of adsorbed oxygen within the temperature range of 150–500 K. Further heating of platinum in oxygen above 500 K results in the formation of "subsurface" oxide, which decomposes at 1250 K [42]. Direct proof of the penetration by oxygen of the near-surface layer of the solid was obtained for Pt(111) by ion scattering [40].

According to electrochemistry research of corrosion processes, the oxygen reduction reaction is a multistep process involving four electron transfers during which bonds are broken and formed, with important involvement of the surrounding water molecules [43]:

$$O_2* + 2H_2O + 4e^- \rightarrow 4OH^- + *, \text{ alkaline medium}, \quad (5)$$

$$O_2* + 4H^+ + 4e^- \rightarrow H_2O_2* + 2H^+ + 2e^- \rightarrow 2H_2O + *, \text{ acidic medium}. \quad (6)$$

Bockris and coworkers [44] have proposed that the adsorption of oxygen atoms arises from an equilibrium of the water discharge reaction with the Pt surface in acidic medium, which usually occurs at 0.6–0.8 V RHE:

$$H_2O + * \rightarrow O* + 2H^+ + 2e^-, \quad (7)$$

whereas in alkaline medium, adsorption of OH^- species is taking place:

$$OH^- + * \rightarrow O* + H^+ + 2e^-. \quad (8)$$

Recently, Harting and Koper [45] proposed in their theoretical study that the rate-determining step in oxygen adsorption is molecular electrosorption, in which one electron is accepted from the metal, as shown in Eq. (2). Depending on the acidity of the solution, this electron transfer is accompanied or followed by a proton transfer to the oxygen, leading to a precursor for hydrogen peroxide formation:

$$O_2 + H^+ + e^- + * \rightarrow HO_2*. \quad (9)$$

In liquid-phase heterogeneous catalysis, which is normally carried out at 293–353 K, it is assumed that oxygen adsorption on Pt occurs via dissociative chemisorption, which may be either reversible [8,28] (Eq. (3)) or irreversible [16,31], as follows:

$$O_2 + 2* \rightarrow 2O*. \quad (10)$$

It can be seen that oxygen adsorption on the metal catalyst can be described by different steps, depending on the temperature, the electrochemical potential, and the pH of the reaction medium.

2.2. Alcohol/aldehyde dehydrogenation

A number of different ways to describe the surface chemistry of the oxidative dehydrogenation mechanism have been proposed [4]. In a pure dehydrogenation mechanism, the rate-determining step is considered to be dehydrogenation of alcohol to the intermediate aldehyde, followed by aldehyde hydration and dehydrogenation to the acid:

$$RCH_2OH* + 2* \rightleftharpoons RCHO* + 2H*, \quad (11)$$

$$RCHO* + H_2O \rightleftharpoons RCH(OH)_2*, \quad (12)$$

$$RCH(OH)_2* + 2* \rightleftharpoons RCOOH* + 2H*. \quad (13)$$

This is in agreement with the observed high rate of aldehyde oxidation in cases where the hydration equilibrium is shifted towards the geminal glycol form and the hydration is catalysed by bases [3,6]. If the glycol formation is negligible, the aldehyde-to-acid transformation is an oxidation reaction. It has also been observed that the oxidation rate for aldehyde increases with increasing pH [11]. Because of their higher nucleophilic property, at high pH, hydroxyl ions rather than water are involved in aldehyde dehydrogenation [38]:

$$RCHO* + OH^- \rightarrow RCOOH* + H^+ + 2e^-. \quad (14)$$

Dijkgraaf et al. have proposed that the dehydrogenation of alcohol starts with proton abstraction, followed by hydride transfer from the carbon atom towards the noble metal surface [26]:

$$RCH_2OH* + OH^- \rightleftharpoons RCH_2O^-* + H_2O, \quad (15)$$

$$RCH_2O^-* + * \rightarrow RCHO* + H^-*. \quad (16)$$

The validity of this step has been disputed, as deprotonation of a very weak acid, such as sugar alcohols, in weakly alkaline medium is rather difficult [46]. Another possibility for this step is hydrogen abstraction from the adsorbed alcohol molecule in two successive steps, assuming that the O–H bond is broken first, forming surface alkoxides [8,15]:

$$RCH_2OH* + * \rightleftharpoons RCH_2O* + H*, \quad (17)$$

$$RCH_2O* + * \rightarrow RCHO* + H*. \quad (18)$$

Recently, Markusse et al. have proposed in their kinetic studies that at high catalyst potentials, the alcohol and aldehyde dehydrogenation steps can be described as irreversible and are accompanied by the production of electrons and protons [31]:

$$RCH_2OH* \rightarrow RCHO* + 2H^+ + 2e^-, \quad (19)$$

$$RCHO* + H_2O \rightarrow RCOOH* + 2H^+ + 2e^-. \quad (20)$$

In electrochemistry, depending on the pH of the medium, the following methanol dehydrogenation steps have been proposed [20]:

- in acidic medium:

$$CH_3OH* \rightarrow CH_3O* + H^+ + e^-, \quad (21)$$

$$CH_3O* \rightarrow CH_2O* + H^+ + e^-; \quad (22)$$

- in alkaline medium:

$$CH_3OH* + OH^- \rightarrow CH_3O* + H_2O + e^-, \quad (23)$$

$$CH_3O* + OH^- \rightarrow CH_2O* + H_2O + e^-. \quad (24)$$

It can be seen that the pH plays a crucial role in the alcohol/aldehyde dehydrogenation step.

2.3. Platinum oxide formation and reduction

It emerges from the dehydrogenation mechanism of alcohol oxidation that the reaction proceeds on free noble metal sites. There is no significant catalyst deactivation while the reactor is operated in a transport-limited regime; that is, the oxygen supply is the rate-determining step and there are free active metal sites present. In batchwise operation, the situation changes after a certain conversion: the surface chemical reaction becomes the rate-determining step because of the lower liquid reactant concentration. This means that the rate of oxygen supply to the catalyst surface is higher than its consumption, which causes successive oxidation of the active metal sites, and the catalyst deactivates. This phenomenon is called overoxidation, which can be seen under oxygen-rich conditions. According to Dijkgraaf et al., adsorbed oxygen atoms on the platinum active metal sites slowly penetrate the skin of the platinum metal (dermasorption) and form a subsurface atom, leading to platinum oxide formation, which finally causes catalyst deactivation [26]. This was considered to be a purely chemical and reversible step [28,47]:

$$O* + *_s \rightleftharpoons O*_s + (*), \quad (25)$$

where $*_s$ denotes adsorption sites for the formation of inactive platinum oxide ($O*_s$), and $(*)$ means free sites that are not available for further adsorption. The simplest way to reduce or reactivate the catalyst is to replace oxygen with nitrogen (inert gas), and then the alcohol reactant reduces the noble metal surface:

$$RCH_2OH* + O*_s \rightarrow RCHO* + H_2O + *_s. \quad (26)$$

Markusse et al. have supported the above mechanism (Eq. (25)) but assumed that formation of the inactive oxide is a purely chemical step, being irreversible, as observed through cyclic voltammetry experiments, whereas reduction of the oxide, an electrochemical step, depends on the catalyst potential [31]:

$$O*_s + H^+ + 2e^- + * \rightarrow OH^- + * + *_s. \quad (27)$$

In electrochemistry, oxide formation is considered a corrosion phenomenon, and it has been proposed that the origin of the oxygen species responsible for the oxide formation is water and not molecular oxygen, which has only one role, which is to increase the catalyst potential [44]. The corrosion process occurs above a potential of 0.8 V RHE, for example, in acidic medium:

$$H_2O + * \rightarrow OH* + H^+ + e^-, \quad (28)$$

whereas in alkaline medium, adsorption of OH^- species is taking place:

$$OH^- + * \rightarrow OH* + e^- \quad (29)$$

followed by

$$OH* \rightarrow O*_s + H^+ + e^-. \quad (30)$$

It can be seen from this section that in heterogeneous catalysis, the oxide formation step has been considered to be pH independent. However, from electrochemistry, it can be concluded that with an increase in pH, the rate of catalyst deactivation due to overoxidation or corrosion increases.

3. Kinetic model

From the above discussions, it is clear that aqueous alcohol oxidation can be described through several mechanisms, which can lead to various kinetic models. It seems complex and difficult to arrive at a general mechanism that can explain all of the phenomena. In recent work Gangwal et al. have demonstrated the versatile nature of the previously developed electrochemical kinetic model of Markusse et al. for alcohol oxidation and catalyst deactivation due to overoxidation [31,33]. However, this model is only suitable for modelling alcohol oxidation at pH 8. It is found that at pH 6, the

Table 1
Reaction steps and rate equations for alcohol oxidation mechanism

Reaction step	Rate equation	
$O_2 + 2* \rightarrow 2O*$	$R_1 = k_1 C_{O_2} \Theta*^2$	(I)
$RCH_2OH + *_\rho \rightleftharpoons RCH_2OH*_\rho$	$\Theta_{RCH_2OH} = K_2 C_{RCH_2OH} \Theta*_\rho$	(II)
$RCHO + *_\rho \rightleftharpoons RCHO*_\rho$	$\Theta_{RCHO} = K_{2a} C_{RCHO} \Theta*_\rho$	(IIa)
$RCH_2OH*_\rho + * \rightarrow RCHO*_\rho + 2H^+ + 2e^- + *$	$R_3 = k_3 \Theta_{RCH_2OH} \Theta* \exp(\frac{EF}{RT})$	(III)
$RCH_2OH*_\rho + * + OH^- \rightarrow RCHO*_\rho + H_2O + H^+ + 2e^- + *$	$R_4 = k_4 \Theta_{RCH_2OH} \Theta* C_{OH} \exp(\frac{EF}{RT})$	(IV)
$RCHO*_\rho + * + H_2O \rightarrow RCOOH*_\rho + 2H^+ + 2e^- + *$	$R_5 = k_5 \Theta_{RCHO} \Theta* \exp(\frac{EF}{RT})$	(V)
$RCHO*_\rho + * + OH^- \rightarrow RCOOH*_\rho + H^+ + 2e^- + *$	$R_6 = k_6 \Theta_{RCHO} \Theta* C_{OH} \exp(\frac{EF}{RT})$	(VI)
$O* + H_2O + 2e^- \rightarrow 2OH^- + *$	$R_7 = k_7 \Theta_o \exp(-\frac{EF}{RT})$	(VII)
$O* + *_s \rightarrow O*_s + *$	$R_8 = k_8 \Theta_o (1 - \Theta_{ox})$	(VIII)
$OH^- + * \rightarrow O*_s + H^+ + 2e^-$	$R_9 = k_9 C_{OH} \Theta* \exp(\frac{EF}{RT})$	(IX)
$RCOOH + *_\rho \rightleftharpoons RCOOH*_\rho$	$\Theta_{RCOOH} = K_{10} C_{RCOOH} \Theta*_\rho$	(X)
$O*_s + H_2O + 2e^- + * \rightarrow 2OH^- + * + *_s$	$R_{11} = k_{11} \Theta_{ox} \Theta* \exp(-\frac{EF}{RT})$	(XI)

model predicts nearly 20 times higher oxidation rates than experimentally observed, whereas at pH 10, the model predicts nearly 20 times lower oxidation rates, compared with pH 8. It is verified by the present experimental work that the model of Markusse et al. fails to describe, qualitatively and quantitatively, the observed pH-dependent reaction rates.

To describe the pH effect, the adopted kinetic mechanism and the reaction rate equations are presented in Table 1. It is assumed that oxygen and the organic compounds (reactant alcohol and the reaction products) adsorb independently. The oxygen adsorption step (I) is considered to be irreversible, as described in Eq. (10). The alcohol reactant adsorption step (II), the intermediate adsorption step (IIa), and the acid product adsorption step (X) are considered to be associative, as assumed by Markusse et al. [31].

The pH effect is assumed to occur through parallel reaction steps: dehydrogenation of alcohol (III and IV), oxidation of aldehyde (V and VI), and platinum oxide formation (VIII and IX). Depending on the pH of the reaction medium, acidic or alkaline, the rate-determining or dominating reaction step will change. Under acidic conditions, step III is the rate-determining step for alcohol dehydrogenation, in accordance with Eqs. (19) and (21), whereas under alkaline conditions, step (IV) is the dominating step (Eq. (23)). For aldehyde oxidation, under acidic conditions, step V is the dominating step (Eq. (20)), whereas under alkaline conditions, step VI is the dominating step (Eq. (14)). It is assumed that strongly adsorbed oxygen is responsible for platinum oxide formation due to overoxidation or corrosion; no discrimination is made between adsorbed oxygen and adsorbed hydroxyl species. Under acidic conditions, step VIII is the dominating oxide formation step, in accordance with Eq. (25), whereas under alkaline conditions, step IX is the dominating step (Eqs. (29) and (30)).

In the present model, the oxygen reduction (VII) and oxide reduction (XI) reaction steps are considered to be independent of pH, in contrast to the model of Markusse et al., which assumes proton concentration dependency [31]. The site balances applied in the present kinetic model are similar to the model of Markusse et al., except for the additional involvement of the aldehyde site coverage, as follows:

alcohol adsorption,

$$\Theta*_\rho + \Theta_{RCH_2OH} + \Theta_{RCHO} + \Theta_{RCOOH} = 1, \tag{31}$$

oxygen adsorption, $$\Theta* + \Theta_o + \Theta_{ox} = 1, \tag{32}$$

subsurface oxygen, $$\Theta*_s + \Theta_{ox} = 1, \tag{33}$$

where $\Theta*_\rho$ is the fraction of the free organic compound adsorption sites, $\Theta*$ is the fraction of the free oxygen adsorption sites, Θ_{ox} is the coverage of inactive oxide formation, and $\Theta*_s$ is the fraction of the oxide formation sites. From Eq. (31) and the equilibrium Eqs. (II), (IIa), and (X) in Table 1, the alcohol coverage fraction is determined as

$$\Theta_{RCH_2OH} = \frac{K_2 C_{RCH_2OH}}{1 + K_2 C_{RCH_2OH} + K_{2a} C_{RCHO} + K_{10} C_{RCOOH}}, \tag{34}$$

where K_i are the equilibrium adsorption parameters defined in Table 7. Similarly, for the intermediate aldehyde and the product acid, the coverage fractions are determined as

$$\Theta_{RCHO} = \frac{K_{2a} C_{RCHO}}{1 + K_2 C_{RCH_2OH} + K_{2a} C_{RCHO} + K_{10} C_{RCOOH}}, \tag{35}$$

$$\Theta_{RCOOH} = \frac{K_2 C_{RCH_2OH}}{1 + K_2 C_{RCH_2OH} + K_{2a} C_{RCHO} + K_{10} C_{RCOOH}}. \tag{36}$$

The surface specific alcohol dehydrogenation rate R_3 (step III, Table 1) increases with increasing free site fraction, $\Theta*$, and consequently decreases with increasing oxygen coverage, Θ_o. Based upon the non-steady-state site balances and the rate equations given in Table 1, the rates of change of oxygen coverage (Θ_o) and oxide coverage (Θ_{ox}) are determined by the following differential equations:

$$\frac{d\Theta_o}{dt} = 2k_1 C_{O_2} \Theta*^2 - k_7 \Theta_o \exp\left(-\frac{EF}{RT}\right) - k_8 \Theta_o (1 - \Theta_{ox}), \tag{37}$$

$$\frac{d\Theta_{ox}}{dt} = k_8 \Theta_o (1 - \Theta_{ox}) + k_9 C_{OH} \Theta* \exp\left(\frac{EF}{RT}\right) - k_{11} \Theta_{ox} \Theta* \exp\left(-\frac{EF}{RT}\right), \tag{38}$$

where k_i are the reaction rate parameters defined in Table 7, C_{O_2} (mol m^{-3}) is the oxygen concentration at the catalyst surface, E (V) is the electrochemical catalyst potential, F (C mol^{-1}) is Faraday's constant, R (J mol^{-1} K^{-1}) is the ideal gas constant, and T (K) is the reaction temperature. The catalyst potential is determined by balancing the rate of electrons produced ($R_3 + R_4 + R_5 + R_6 + R_9$) per volume of catalyst and the rate of electrons consumed ($R_7 + R_{11}$) per volume of catalyst as

$$E = \frac{RT}{2F} \ln\left(\frac{R_{\text{oxid1}} + R_{\text{oxid2}}}{R_{\text{red1}} + R_{\text{red2}} + R_{\text{red3}} + R_{\text{red4}} + R_{\text{red5}}}\right), \quad (39)$$

where R_i are the reaction rates of species i, defined in Table 1, and

$$R_{\text{red1}} = k_3 L_t \rho_p \Theta_{\text{RCH}_2\text{OH}} \Theta *, \quad (40)$$

$$R_{\text{red2}} = k_4 L_t \rho_p C_{\text{OH}} \Theta_{\text{RCH}_2\text{OH}} \Theta *, \quad (41)$$

$$R_{\text{red3}} = k_5 L_t \rho_p \Theta_{\text{RCHO}} \Theta *, \quad (42)$$

$$R_{\text{red4}} = k_6 L_t \rho_p C_{\text{OH}} \Theta_{\text{RCHO}} \Theta *, \quad (43)$$

$$R_{\text{red5}} = k_9 L_t \rho_p C_{\text{OH}} \Theta *, \quad (44)$$

$$R_{\text{oxid1}} = k_7 L_t \rho_p \Theta_o, \quad (45)$$

$$R_{\text{oxid2}} = k_{11} L_t \rho_p \Theta_{ox} \Theta *, \quad (46)$$

where k_i are the reaction rate parameters defined in Table 7, L_t is the weight-specific number of platinum surface atoms (i.e., mol$_{\text{Pt}_s}$ kg$_{\text{cat}}^{-1}$), based on the assumption that one Pt surface atom equals one catalytic site, and ρ_p is the catalyst particle density. It should be noted that two important phenomena limit the range of the catalyst potential. First, below a potential of 0.4 V RHE, hydrogen gas evolves, because of water reduction, and CO formation is possible. Second, above a potential of 1.5 V RHE, oxygen gas evolves, because of water oxidation. Since these reactions are not taken into account in the kinetic model presented in Table 1, Eq. (39) can be applied only if

$$0.4 \text{ V RHE} < E < 1.5 \text{ V RHE}. \quad (47)$$

The overall volumetric rate of consumption of oxygen, $R_{\text{v,O}_2}$ (mol m^{-3} s^{-1}), is dependent on the amount of oxygen present at the catalyst surface as well as on the activity of the catalyst. Therefore, from Eq. (I) of Table 1,

$$R_{\text{v,O}_2} = L_t C_{\text{cat}} k_1 \Theta *^2 C_{o_2}, \quad (48)$$

where C_{cat} is the catalyst concentration. The weight-specific dehydrogenation rate of the reactant alcohol, $R_{\text{RCH}_2\text{OH}}$ (mol kg^{-1} s^{-1}), from Eqs. (III) and (IV) of Table 1, can be determined as

$$R_{\text{RCH}_2\text{OH}} = L_t (k_3 + k_4 C_{\text{OH}}) \Theta_{\text{RCH}_2\text{OH}} \Theta * \exp\left(\frac{EF}{RT}\right). \quad (49)$$

The weight-specific acid formation rate, R_{RCOOH} (mol kg^{-1} s^{-1}), which is measured through the rate of alkali (NaOH) addition, can be calculated from the rate of aldehyde oxidation (Eqs. (V) and (VI) of Table 1) as

$$R_{\text{RCOOH}} = L_t (k_5 + k_6 C_{\text{OH}}) \Theta_{\text{RCHO}} \Theta * \exp\left(\frac{EF}{RT}\right). \quad (50)$$

Table 2
Catalyst properties

Catalyst property	Pt/Gr (Vleeming et al. [28])	Pt/C (Engelhard, code-43545)	Pt/Gr (Johnson Matthey, JM287)
Dispersion (%)	43	42	15
BET surface area (m^2 g^{-1})	102	900	15
Pt content (wt%)	3.3	5	5
Particle size (μm)	15	35–40	15
Moisture content (%)	Dry	46.88	Dry
Porosity (%)	40	80	40
Density (kg m^{-3})	1350	1050	1350

4. Experimental

In this work, experiments were performed in a stirred three-phase semi-batch reactor. The aqueous alcohol methyl α-D-glucopyranoside (MGP) is added in a batch mode. The gaseous oxidant (molecular oxygen) is supplied continuously by a mass flow controller. The oxygen partial pressure is set by the nitrogen flow, also supplied by a mass flow controller. The pH is monitored and kept at a constant level by controlled addition of a 0.1 M NaOH solution. During the reaction, the liquid reactant is converting to the product with time, that is, MGP gives 1-O-methyl α-D-glucuronic acid (MG) with methyl α-D-6-aldehydo-glucopyranoside (MAGP) as the intermediate. The acid formation rate is measured through the rate of addition of alkali. The oxygen concentration in the liquid phase is measured with an oxygen electrode. The open-circuit electrochemical catalyst potential is measured with a smooth Pt wire as a working electrode and Ag/AgCl, saturated KCl, as a reference electrode.

Two commercial nonuniform (egg shell) catalysts, a 5 wt% Pt on carbon (Engelhard, code-43545) and a 5 wt% Pt on graphite (Johnson Matthey, JM287), were used. The properties of the catalysts are presented in Table 2. The pH of the reaction medium is the only parameter that differs between the experiments. Experiments were performed under the set of reaction conditions presented in Table 3; the procedure is described elsewhere [33].

5. Kinetic parameter estimation

The goal of this work is to obtain a dynamic electrochemical model with a set of kinetic parameters that can adequately describe the observed experimental data, at different pH conditions for the catalyst with different supports and metal dispersion. To avoid strong interdependence and mutual correlation of the parameters and to achieve a reliable parameter estimation, we obtained the kinetic parameters of the model described in Section 3 in two consecutive steps. First, pH-independent parameters (k_1, K_2, k_3, k_7, k_8, and K_{10}) are estimated, which are then further used for the estimation of pH-dependent parameters (k_4, k_5, k_6, and k_9).

Table 3
Experimental operating conditions

Operating condition	CSTR (Vleeming et al. [28])	Semi-batch reactor
pH (−)	8	6–10
Degree of conversion (%)	3–47	5–40
Temperature, T (K)	323	323
Catalyst concentration, C_{cat} (kg m^{-3})	2	2
Stirring speed (rpm)	1000	1000
Oxygen partial pressure, P_{O_2} (kPa)	10–100	40
Initial MGP concentration, C_{MGP} (mol m^{-3})	11–427	100
Initial MG concentration, C_{MG} (mol m^{-3})	1.5–41	0
Liquid volume, V_L (m^3)	0.35×10^{-3}	0.5×10^{-3}
Gas volume, V_G (m^3)	0.2	0.35
Volumetric gas flow, F_G (m^3 s^{-1})	5×10^{-6}	14×10^{-6}
Gas-to-liquid mass transport coefficient, $k_{GL}a_{GL}$ (s^{-1})	0.4	0.4

5.1. pH-independent kinetic parameters

The pH-independent kinetic parameters are estimated from a set of 12 experiments performed in a CSTR with Pt on graphite catalyst (43% dispersion). The catalyst properties and experimental conditions are presented in Tables 2 and 3, respectively. Each experiment is performed at a constant pH of 8 and contains 40 reaction rate data measured at a constant conversion level. The details of the experimental procedure are described elsewhere [28]. It was verified that all data were obtained under intrinsic kinetic conditions, except for data obtained at a partial pressure of 10 kPa, which represent the effect of gas-to-liquid mass transport limitation [32].

The kinetic model presented in Table 1 is simplified with the help of the following assumptions to account for the constant pH:

- The intermediate aldehyde disappearance, step (V), is very fast; that is, the rates of the disappearance of the aldehyde (Eq. (42)) and of the alcohol (Eq. (40)) can be considered equal: $R_{red3} = R_{red1}$.
- The hydroxyl concentration-dependent steps (IV), (VI), and (IX) are considered insignificant because experimental data are available at sufficiently low pH (pH 8). This means $R_{red2} \ll R_{red1}$, $R_{red4} \ll R_{red1}$, and $R_{red5} \ll R_{red1}$.

With the above assumptions, the catalyst potential equation (Eq. (39)) can be rewritten as

$$E = \frac{RT}{2F} \ln\left(\frac{R_{oxid1} + R_{oxid2}}{2R_{red1}}\right), \tag{51}$$

which then leads to

$$\exp\left(\frac{EF}{RT}\right) = \left(\frac{k_7\Theta_o + k_{11}\Theta_{ox}\Theta*}{2k_3\Theta_{RCH_2OH}\Theta*}\right)^{\frac{1}{2}} \tag{52}$$

and

$$\exp\left(-\frac{EF}{RT}\right) = \left(\frac{2k_3\Theta_{RCH_2OH}\Theta*}{k_7\Theta_o + k_{11}\Theta_{ox}\Theta*}\right)^{\frac{1}{2}}. \tag{53}$$

Substitution of Eqs. (52) and (53) in Eqs. (37), (38), and (49) results in

$$\frac{d\Theta_o}{dt} = 2k_1 C_{O_2}\Theta*^2 - k_7\Theta_o\left(\frac{2k_3\Theta_{RCH_2OH}\Theta*}{k_7\Theta_o + k_{11}\Theta_{ox}\Theta*}\right)^{\frac{1}{2}} - k_8\Theta_o(1-\Theta_{ox}), \tag{54}$$

$$\frac{d\Theta_{ox}}{dt} = k_8\Theta_o(1-\Theta_{ox}) - k_{11}\Theta_{ox}\Theta*\left(\frac{2k_3\Theta_{RCH_2OH}\Theta*}{k_7\Theta_o + k_{11}\Theta_{ox}\Theta*}\right)^{\frac{1}{2}}, \tag{55}$$

$$R_{RCH_2OH} = L_t k_3\Theta_{RCH_2OH}\Theta*\left(\frac{k_7\Theta_o + k_{11}\Theta_{ox}\Theta*}{2k_3\Theta_{RCH_2OH}\Theta*}\right)^{\frac{1}{2}}. \tag{56}$$

It turns out that these simplified model equations resemble the kinetic model equations of Markusse et al. [31]. In previous work, it was found that some of the kinetic parameters of this model, especially k_3 and k_7, are highly correlated (approximate correlation > 0.9) [48]. For the reliable estimation of these parameters, the lumped parameters $(k_3k_7)^{\frac{1}{2}}$ and $(k_3k_{11})^{\frac{1}{2}}$ are identified, which can be recognised in Eqs. (54), (55), and (56). In addition, to include the measured reaction rate data at an oxygen partial pressure of 10 kPa and initial reaction conditions, the influence of gas-to-liquid mass transport limitation has to be accounted for in the model for accurate parameter estimation [48]. The mass transport equations must be considered are as follows:

Gas phase (G) mass balance.

Oxygen mass transport from the gas phase to the liquid phase:

$$\frac{V_G}{RT}\frac{dP_{O_2}}{dt} = \frac{F_G(P^{in}_{O_2} - P_{O_2})}{RT} - k_{GL}a_{GL}V_L(HP_{O_2} - C_{O_2,L}), \tag{57}$$

where V_G (m^3) is the volume of gas in the reactor, P_{O_2} (kPa) is the oxygen partial pressure in the reactor, F_G (m^3 s^{-1}) is the total volumetric gas flow rate, $k_{GL}a_{GL}$ (s^{-1}) is the volumetric gas-to-liquid mass transport coefficient, H (mol m^{-3} Pa^{-1}) is the Henry coefficient, and $C_{O_2,L}$ (mol m^{-3}) is the oxygen concentration in the liquid phase.

Table 4
Kinetic parameters with their individual 95% confidence intervals and correlation matrix, obtained with initial rate (after 50 s) data of MGP oxidation in CSTR

Parameter	Reaction step	Pt/Gr (dispersion 43%)	Correlation matrix			
k_1 ($m^3\,mol^{-1}\,s^{-1}$)	Oxygen adsorption	(1.76 ± 4.30)	1	0.16	0.06	−0.11
K_2 ($m^3\,mol^{-1}$)	Alcohol adsorption	$(6.51 \pm 8.60) \times 10^{-3}$	0.16	1	0.43	−0.83
K_{10} ($m^3\,mol^{-1}$)	Acid adsorption	$(9.75 \pm 13.67) \times 10^{-2}$	0.06	0.43	1	0.10
$(k_3k_7)^{\frac{1}{2}}$ (s^{-1})	Alcohol oxidation	$(1.58 \pm 0.66) \times 10^{-1}$	−0.11	−0.83	0.10	1

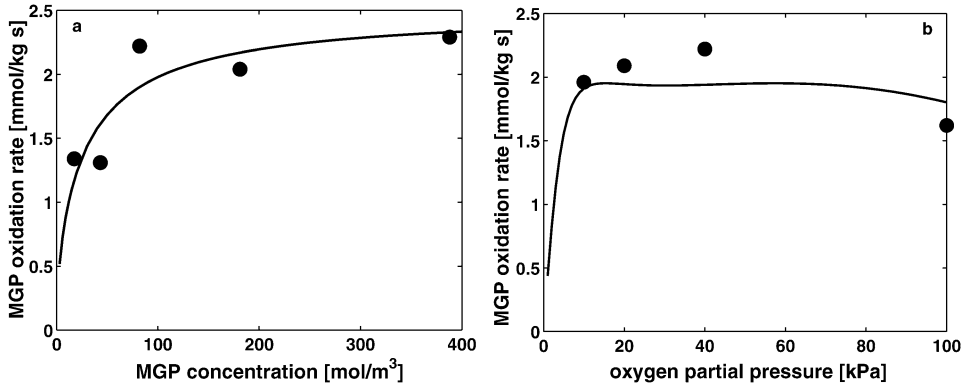

Fig. 1. Effect of (a) MGP concentration and (b) oxygen partial pressure, on experimental (symbols) and model predicted (solid lines), MGP oxidation rates obtained after 50 s. Data used: (a) $P_{O_2} = 40$ kPa, $L_t = 0.073$ mol kg_{cat}^{-1} and (b) $C_{MGP} = 90$ mol m^{-3}, $C_{MG} = 10$ mol m^{-3}, $L_t = 0.073$ mol kg_{cat}^{-1}.

Liquid phase (L) mass balance.

Oxygen mass transport from the liquid phase to the solid phase:

$$V_L \frac{dC_{O_2,L}}{dt} = k_{GL} a_{GL} V_L (H P_{O_2} - C_{O_2,L}) - R_{v,O_2}, \qquad (58)$$

where V_L (m^3) is the total liquid volume and R_{v,O_2} is the overall volumetric oxygen consumption rate, determined by Eq. (48).

A generalised nonlinear least-squares routine of MATLAB, which uses the Levenberg–Marquardt algorithm [49], is used for the optimisation. The residual sum of squares that is minimised is

$$\text{resid}_{CSTR} = \Sigma (R_{RCH_2OH,t\,(model)} - R_{RCH_2OH,t\,(exp)})^2. \qquad (59)$$

The regression analysis is performed in two parts. First, the initial oxidation rate data (after 50 s) are used to obtain estimates for the parameters of the initial rate model. Next, the regression analysis is extended to the entire oxidation rate data in the time interval between 50 and 10 000 s, in which all parameters are estimated simultaneously.

5.1.1. Initial oxidation rate data

For the regression analysis, it is assumed that the catalyst deactivation due to overoxidation is absent, that is, $\Theta_{ox} = 0$. Hence, the oxide formation (step (VIII)) and oxide reduction (step (XI)) can be eliminated from the model. The reversible steps (II) and (X) are considered to be in quasi-equilibrium. Eq. (51) then simplifies to

$$E = \frac{RT}{2F} \ln\left(\frac{R_{oxid1}}{2R_{red1}}\right), \qquad (60)$$

which leads to

$$\exp\left(\frac{EF}{RT}\right) = \left(\frac{k_7 \Theta_o}{2k_3 \Theta_{RCH_2OH} \Theta*}\right)^{\frac{1}{2}}. \qquad (61)$$

Substitution of the above equation in Eqs. (37) and (49) results in

$$\frac{d\Theta_o}{dt} = 2k_1 C_{O_2} \Theta*^2 - (k_3k_7)^{\frac{1}{2}} (2\Theta_{RCH_2OH} \Theta* \Theta_o)^{\frac{1}{2}}, \qquad (62)$$

$$R_{RCH_2OH} = L_t (k_3k_7)^{\frac{1}{2}} (0.5\Theta_{RCH_2OH} \Theta* \Theta_o)^{\frac{1}{2}}. \qquad (63)$$

For the parameter estimation, the kinetic model Eqs. (62) and (63) are solved in combination with the gas-to-liquid mass transport Eqs. (57) and (58). The regression analysis is performed with experimental data obtained after 50 s. The estimated kinetic parameters, along with their confidence intervals, are presented in Table 4. The confidence intervals for the first three parameters (k_1, K_2, and K_{10}) are quite wide, which suggests that the measured data available for the regression analysis are not sufficient and the parameter estimates are preliminary. The fitting of the model is illustrated in Figs. 1a and 1b, which shows the effects of MGP concentration and oxygen partial pressure, respectively, on the initial oxidation rate. It is found that the kinetic parameters obtained in previous work [48] are present within the confidence interval of newly estimated parameters. The correlation matrix, which gives an indication of the degree of interdependence between the estimated parameters, is also presented in Table 4. The mutual correlation between the parameters is low, except that between parameters $(k_3k_7)^{\frac{1}{2}}$ and K_2, which corresponds to 0.83. This can be explained by the structure of the model, since substitution of Eq. (34)

Table 5
Kinetic parameters with their individual 95% confidence intervals and correlation matrix, obtained with the rate data, in the interval of 50–10 000 s, of MGP oxidation in CSTR

Parameter	Reaction step	Pt/Gr (dispersion 43%)	Correlation matrix					
k_1 ($m^3\,mol^{-1}\,s^{-1}$)	Oxygen adsorption	$(9.11 \pm 0.94) \times 10^{-1}$	1	0.10	0.09	0.15	−0.39	−0.13
K_2 ($m^3\,mol^{-1}$)	Alcohol adsorption	$(8.50 \pm 1.00) \times 10^{-3}$	0.10	1	0.53	−0.73	−0.01	0.13
K_{10} ($m^3\,mol^{-1}$)	Acid adsorption	$(1.29 \pm 0.16) \times 10^{-1}$	0.09	0.53	1	0.03	−0.07	0.03
$(k_3k_7)^{\frac{1}{2}}$ (s^{-1})	Alcohol oxidation	$(1.64 \pm 0.06) \times 10^{-1}$	0.15	−0.73	0.03	1	0.22	0.01
(k_8) (s^{-1})	Oxide formation	$(1.15 \pm 0.08) \times 10^{-3}$	−0.39	−0.01	−0.07	0.23	1	0.66
$(k_3k_{11})^{\frac{1}{2}}$ (s^{-1})	Oxide reduction	$(5.61 \pm 3.54) \times 10^{-5}$	−0.13	0.13	0.03	0.01	0.66	1

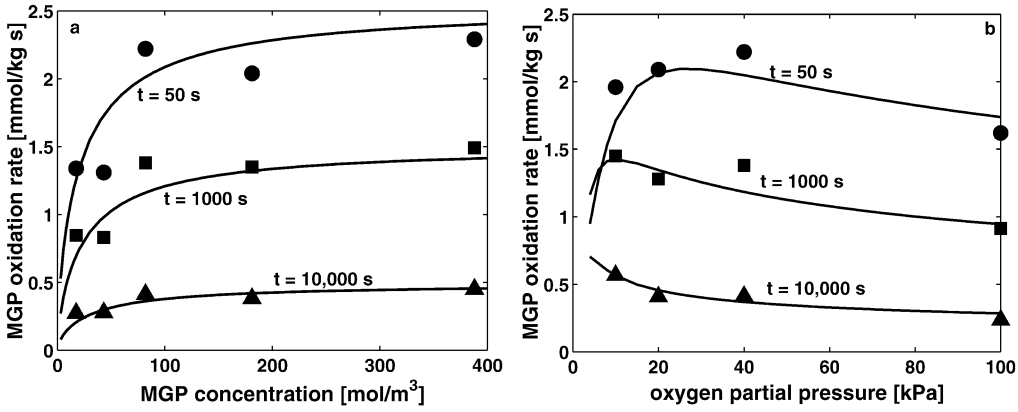

Fig. 2. Effect of (a) MGP concentration and (b) oxygen partial pressure, on experimental (symbols) and model predicted (lines) MGP oxidation rates obtained in time interval of 50–10 000 s. Data used: (a) $P_{O_2} = 40$ kPa, $L_t = 0.073$ mol kg_{cat}^{-1}, and (b) $C_{MGP} = 90$ mol m^{-3}, $C_{MG} = 10$ mol m^{-3}, $L_t = 0.073$ mol kg_{cat}^{-1}.

in Eq. (56) shows that the rate is mainly determined by the product of $(k_3k_7)^{\frac{1}{2}}$ and $K_2{}^{\frac{1}{2}}$.

5.1.2. Oxidation rate data including deactivation

The initial kinetic parameters, presented in Table 4, are used as starting values for the parameter estimation with entire oxidation data, $t > 50$ s. The model predictions are obtained with the use of gas-to-liquid mass transport Eqs. (57) and (58) and kinetic Eqs. (54), (55), and (56). For the parameter estimation the kinetic equations are simplified. It is assumed that during alcohol oxidative dehydrogenation in the presence of oxygen, the catalyst potential is mainly determined by the oxygen reduction (R_{oxid1}) and alcohol dehydrogenation (R_{red1}) reactions (i.e., in Eq. (51), $R_{oxid1} \gg R_{oxid2}$). However, with respect to catalyst reactivation by oxide removal, the catalyst potential is determined by oxide reduction (R_{oxid2}) and alcohol dehydrogenation (R_{red1}), since oxygen is removed and Θ_o quickly becomes very low. This means that in Eq. (51), $R_{oxid2} \gg R_{oxid1}$. The estimated kinetic parameters, along with their confidence intervals, are presented in Table 5. The kinetic parameters are obtained within the confidence interval of the initial kinetic parameters of Table 4. The correlation matrix is also presented in Table 5. The mutual correlation between the same parameters as discussed in the previous section is low, and maximum correlation amounts to only 0.73. Figs. 2a and 2b show the effects of MGP concentration and oxygen partial pressure on the rate of oxidation and catalyst deactivation, respectively. It can be seen that the model with the estimated kinetic parameters describes the observed experimental data well.

5.1.3. Modelling catalyst reactivation

Vleeming et al. showed that the catalyst activity can be recovered by reduction of the catalyst in situ, by shutoff of the oxygen supply, for about 1000 s [28]. However, because of insufficient information on experimentally observed reactivation times, an insignificant oxide reduction parameter $(k_3k_{11})^{\frac{1}{2}}$ is obtained, as presented in Table 5. To model the experimentally observed catalyst reactivation times, the parameter estimation is repeated, but this time the individual oxide reduction parameter, k_{11}, is used. The value of this parameter is selected from previous work [48] and kept fixed ($k_{11} = 1.50 \times 10^3$ s^{-1}), while the rest of the parameters are reestimated. It is found that the adsorption parameters, k_1, K_2 and K_{10}, remain unchanged. However, new estimates for k_3, k_8, and k_7 are obtained, as presented in Table 6. It should be noted that during regression the lumped parameter $(k_3k_7)^{\frac{1}{2}}$ remains the same. The results of the model simulations for catalyst deactivation and subsequent reactivation, which is known as the redox cycle, are shown in Figs. 3a and 3b. The details of the model simulation procedure for the redox cycle can be found elsewhere [32]. The oxide reduction parameter (k_{11}) can be safely used within the range of $(1.5–2.2) \times 10^3$ s^{-1} with corresponding reactivation times of

Table 6
Kinetic parameters with their individual 95% confidence intervals for the catalyst reactivation of MGP oxidation in CSTR

Parameter	Reaction step	Pt/Gr (dispersion 43%)
k_3 (s^{-1})	Alcohol dehydrogenation	$(5.28 \pm 3.02) \times 10^{-9}$
k_7 (s^{-1})	Oxygen reduction	$(5.10 \pm 2.96) \times 10^{6}$
k_8 (s^{-1})	Oxide formation	$(1.13 \pm 0.08) \times 10^{-3}$
k_{11} (s^{-1})	Oxide reduction	1.5×10^{3}

1349–1574 s, which is close to the experimentally observed reactivation time of 1000 s [28].

5.2. pH dependent kinetic parameters

For the estimation of the pH-dependent parameters, a set of six experiments performed in a semi-batch reactor with two different catalysts, Pt on carbon (42% dispersion) and Pt on graphite (15% dispersion), is used. Each experiment contains 10 acid formation rate data obtained under different pH conditions. The catalyst properties and experimental conditions are presented in Tables 2 and 3, respectively. Furthermore, the complete kinetic model presented in Table 1 is used. To avoid overparameterisation, and depending on the type of catalyst used, the kinetic parameters, estimated and discussed in the previous section, are kept fixed or are adjustable, as shown in Table 7. For example, in the case of the carbon-supported Pt catalyst, the adsorption parameters of the organic reactants (K_2 and K_{2a}) are kept adjustable, while the acid product adsorption parameter (K_{10}) is kept fixed. It is found that as a result of stronger adsorption for organic reactants, the carbon-supported catalyst gives a higher initial rate of reaction as compared with the graphite-supported catalyst [48]. In the case of the graphite-supported Pt catalyst, the adsorption parameters are kept fixed while the oxygen

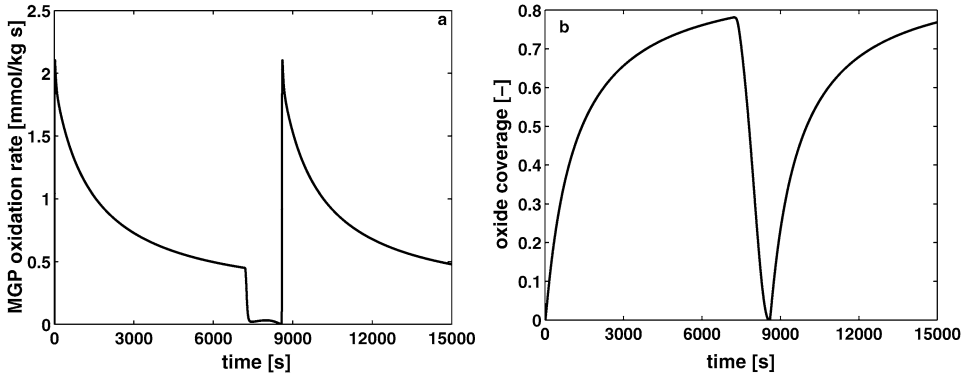

Fig. 3. Simulated (a) specific rate of consumption of MGP and (b) oxide coverage, to illustrate catalyst deactivation and reactivation by removing oxygen, on MGP oxidation rates. Data used: $P_{O_2} = 40$ kPa, $L_t = 0.073$ mol kg_{cat}^{-1}, $C_{MGP} = 90$ mol m^{-3}, $C_{MG} = 10$ mol m^{-3}, and $P_{O_2} = 0$ after 7200 s.

Table 7
Kinetic parameter estimates with their individual 95% confidence intervals by regression of experimental data obtained at pH = 6–10 and $T = 323$ K, for MGP oxidation in semi-batch reactor

Parameter	Reaction step	Pt/C (dispersion 42%)	Pt/Gr (dispersion 15%)
k_1 ($m^3\,mol^{-1}\,s^{-1}$)	Oxygen adsorption	9.10×10^{-1} (fixed)	9.10×10^{-1} (fixed)
K_2 ($m^3\,mol^{-1}$)	Alcohol adsorption	$(5.78 \pm 2.30) \times 10^{-2}$	8.50×10^{-3} (fixed)
K_{2a} ($m^3\,mol^{-1}$)	Aldehyde adsorption	$(5.78 \pm 2.30) \times 10^{-2}$	8.50×10^{-3} (fixed)
K_{10} ($m^3\,mol^{-1}$)	Acid adsorption	1.29×10^{-1} (fixed)	1.29×10^{-1} (fixed)
k_3 (s^{-1})	Alcohol dehydrogenation	5.28×10^{-9} (fixed)	5.28×10^{-9} (fixed)
k_4 ($m^3\,mol^{-1}\,s^{-1}$)	Alcohol dehydrogenation (pH)	$(3.40 \pm 0.62) \times 10^{-4}$	$(5.80 \pm 4.72) \times 10^{-4}$
k_5 (s^{-1})	Aldehyde dehydrogenation	$(4.88 \pm 1.72) \times 10^{-7}$	$(6.42 \pm 6.88) \times 10^{-8}$
k_6 ($m^3\,mol^{-1}\,s^{-1}$)	Aldehyde dehydrogenation (pH)	1.60 ± 1.18	3.68 ± 5.08
k_7 (s^{-1})	Oxygen reduction	5.10×10^{6} (fixed)	$(4.57 \pm 1.28) \times 10^{7}$
k_8 (s^{-1})	Oxide formation	1.13×10^{-3} (fixed)	1.13×10^{-3} (fixed)
k_9 ($m^3\,mol\,s^{-1}$)	Oxide formation (pH)	$(9.39 \pm 3.44) \times 10^{-7}$	$(6.0 \pm 6.06) \times 10^{-7}$
k_{11} (s^{-1})	Oxide reduction	1.50×10^{3} (fixed)	1.50×10^{3} (fixed)

reduction parameter is kept adjustable because of the lower dispersion, that is, larger Pt crystallites compared with the carbon-supported Pt catalyst. Throughout it is assumed that the aldehyde adsorption parameter is of the same magnitude as the alcohol adsorption parameter. This is acceptable because aldehyde and alcohol have nearly equal molar masses, and they are assumed to be adsorbed in a similar manner. The complete kinetic model, combined with mass transport equations, is implemented in a laboratory-scale semi-batch reactor model for the estimation of the kinetic parameters. The residual sum of squares that is minimised with the Levenberg–Marquardt algorithm is

$$\text{resid}_{\text{semi-batch}} = \Sigma(R_{\text{RCOOH},t\,(\text{model})} - R_{\text{RCOOH},t\,(\text{exp})})^2. \quad (64)$$

The estimates of the kinetic parameters, along with their confidence intervals, are presented in Table 7. The estimated mutual correlation between the parameters is found to be low, and the maximum correlation obtained is only 0.74. Examples of fitting results of the complete model are discussed and compared with experimental data in Sections 5.2.1 and 5.2.2. It can be seen from Table 7 that for the Pt on carbon catalyst, adsorption parameters (K_2 and K_{2a}) of the organic reactants are estimated to be nearly 5 to 7 times higher compared with the graphite-supported Pt catalyst. In addition, the overall ($k_5 + k_6 C_{\text{OH}}$) aldehyde disappearance rate parameter is estimated to be two orders of magnitude higher than the overall ($k_3 + k_4 C_{\text{OH}}$) alcohol dehydrogenation rate parameter at pH > 7. This has also been shown experimentally by Schuurman et al. [8].

For the graphite-supported Pt catalyst (15% dispersion), which has a lower dispersion compared with the carbon-supported Pt catalyst (42% dispersion), an oxygen reduction parameter (k_7) that is nearly 10 times higher is obtained. This can be a consequence of the decrease in the oxygen adsorption enthalpy [50], or the increase in the electrochemical reduction rate of oxygen at platinum electrodes [51,52], due to larger metal crystallites.

5.2.1. MGP oxidation with Pt on carbon catalyst

Fig. 4a shows the acid formation rate as a function of time for the eggshell type of Pt on carbon catalyst under different pH conditions. The rate of acid formation increases with increasing pH. It can also be seen that with increasing pH the rate of catalyst deactivation increases. To understand the observed catalyst deactivation, the catalyst potential against time is presented in Fig. 4b. The catalyst potential increases with increasing pH. It can be seen that starting from a reduced catalyst (0.1 V potential) surface, the catalyst potential instantly increases to 0.83 V for pH 6 and 0.93 V for pH 8 and 10, as soon as the oxygen reaches the catalyst surface and stabilises to higher level, around 0.87 V for pH 6, 0.97 V for pH 8, and 0.99 V for pH 10. This indicates that the catalyst deactivates very fast, because of a high oxide coverage, with increasing pH.

Fig. 4a shows that the developed model, with the rate constants as given in Table 7, is well able to describe the observed reaction rates under different pH conditions. The increase in the reaction rate with increasing pH is followed by strong catalyst deactivation caused by overoxidation. The deactivation due to overoxidation can also be seen through the simulated oxide coverage against time in Fig. 4c. After 5000 s, at pH 6, approximately 70% ($\Theta_{\text{ox}} = 0.7$), whereas at pH 10, approximately 80% ($\Theta_{\text{ox}} = 0.8$) of the catalyst surface is covered with inactive platinum oxide. This means with increasing pH from 6 to 10, the rate of catalyst deactivation due to overoxidation increases by approximately 10%, as indicated by the oxide coverage.

Fig. 4d shows the simulated intermediate aldehyde concentration against time. The aldehyde concentration decreases with increasing pH of the reaction medium. Under the present conditions the maximum aldehyde concentration obtained is around 1 mol m^{-3} at pH 6, and it decreases to approximately 0.02 mol m^{-3} at pH 10. Fig. 4e shows the simulated oxygen coverage with time. It can be seen that the initial oxygen coverage decreases with increasing pH, and a maximum coverage of around 0.6 is observed at pH 6.

Fig. 4f shows the simulated concentration of the reactant alcohol, MGP, as a function of time. It can be seen that at lower pH the calculated conversion, from MGP concentration data, is around 25% over the 5000-s period of the reaction. Within this conversion, it can be accepted that the MGP oxidation displays close to 100% selectivity, whereas at the higher pH 10, the conversion is 40%, at which the experimentally observed selectivity is close to 90%. It was verified that carbon balance does not deviate significantly from 100% and the alkali consumption is completely accounted for by the total amount of carboxylic anions analysed [11]. Considering these facts and the model performance, it can be said that the developed model accurately describes the observed pH effect on MGP oxidation.

It should be noted that Schuurman et al. also found that the rate of MGP oxidation increases linearly with increasing pH above 8.5, whereas at low pH, between pH 6 and 8, no difference in the oxidation rates was observed [8]. This latter observation is also verified through model simulation, showing that at pH 6 and 8, there is no difference in the MGP oxidation rates, which can be seen from MGP conversion (Fig. 4f). However, it is noted that the acid formation rate presented in Fig. 4a is a measure of the aldehyde disappearance rate and hence shows slight differences in the initial rates at pH 6 and 8. This effect can also be seen from the change in the aldehyde concentrations, presented in Fig. 4d. The rate of aldehyde disappearance increases with increasing pH. A similar observation has been reported in the literature [11,53]. The observed catalyst deactivation with increasing pH is a well-known phenomenon in electrochemistry that is referred to as corrosion [41,44]. This suggests that the oxygen species responsible for the high oxide coverage at pH 10 originates from hydroxyl species.

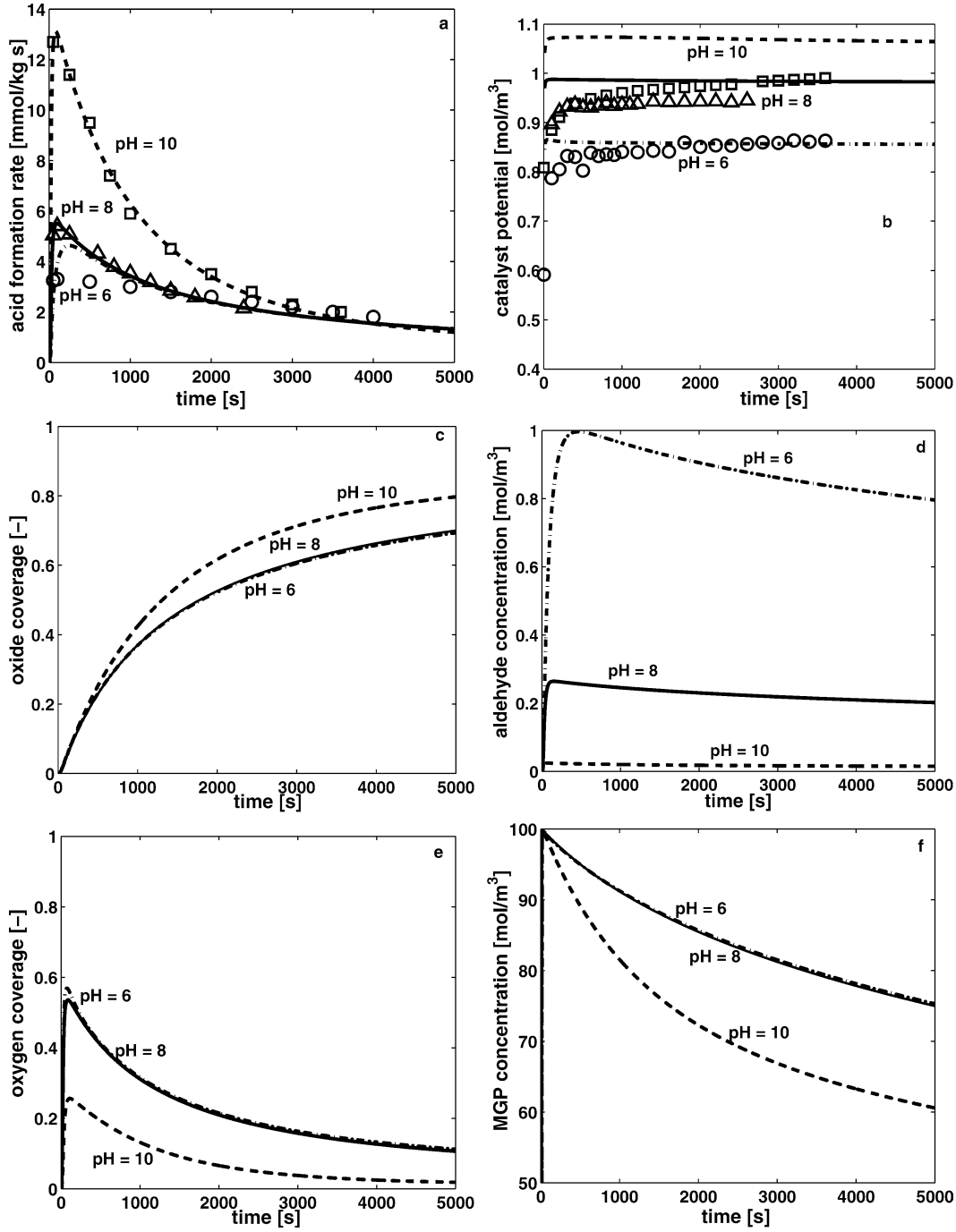

Fig. 4. Effect of pH on: (a) the acid formation rate; (b) the electrochemical catalyst potential; (c) the platinum oxide coverage; (d) the intermediate aldehyde concentration; (e) the oxygen coverage; (f) the alcohol reactant MGP concentration, during Pt/carbon catalysed MGP oxidation. Symbols represent experimental data, i.e. circles for pH = 6, triangles for pH = 8, and squares for pH = 10, whereas lines represent modelling results, i.e. dashed–dotted line for pH = 6, continuous line for pH = 8, and dashed line for pH = 10. Data used: $P_{O_2} = 40$ kPa, $L_t = 0.0385$ mol kg_{cat}^{-1}, and $C_{MGP,ini} = 100$ mol m^{-3}.

5.2.2. MGP oxidation with Pt on graphite catalyst

Fig. 5a shows the acid formation rate as a function of time for the eggshell type of Pt on graphite catalyst at different pH. It can be seen from the experimental results that the initial rate of reaction increases with increasing pH, similar to the carbon-supported catalyst. However, the reaction rates are nearly two times lower compared with the carbon-supported Pt catalyst. Fig. 5b shows the measured catalyst potentials as a function of time. It can be seen that for the graphite-supported catalyst, with increasing pH, the potential increases along with the increase in the reaction rate, but the rate of catalyst deactivation due to overoxidation also increases.

It can be seen that starting from a reduced catalyst (0.1 V potential) surface, the catalyst potential instantly increases to 0.8 V for pH 6 and 0.9 V for pH 8 and 9, as soon as

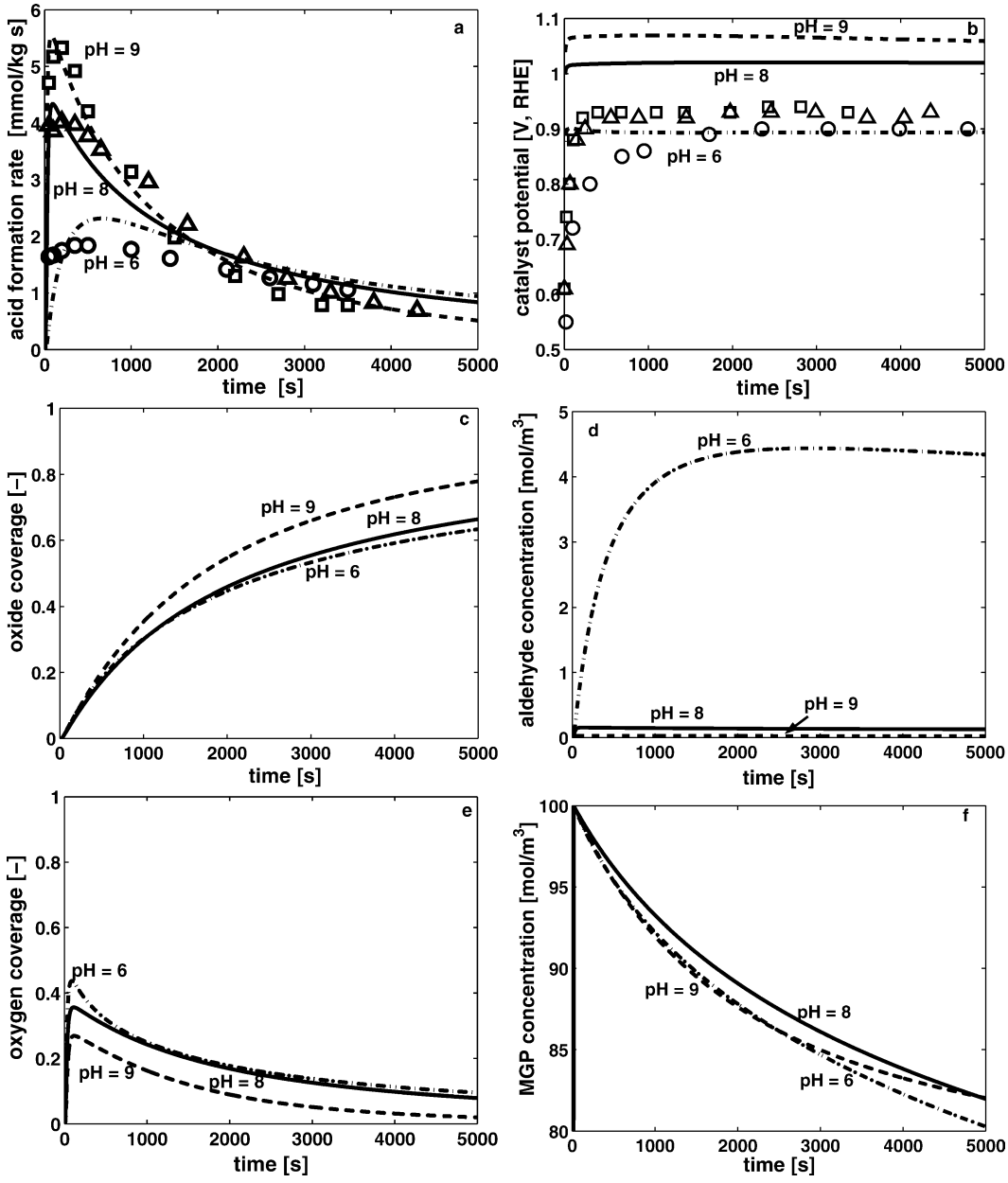

Fig. 5. Effect of pH on: (a) the acid formation rate; (b) the intermediate aldehyde concentration; (c) the platinum oxide coverage; (d) the electrochemical catalyst potential; (e) the oxygen coverage; (f) the reactant MGP concentration, during Pt/graphite catalysed MGP oxidation. Symbols represent experimental data, i.e. circles for pH = 6, triangles for pH = 8, and squares for pH = 9, whereas lines represent modelling results, i.e. dashed–dotted line for pH = 6, continuous line for pH = 8, and dashed line for pH = 9. Data used: $P_{O_2} = 40$ kPa, $L_t = 0.1077$ mol kg_{cat}^{-1}, and $C_{MGP,ini} = 100$ mol m^{-3}.

the oxygen reaches the catalyst surface and stabilises to a higher level, around 0.91 V for pH 6 and around 0.94 V for pH 8 and pH 9. This increase in potential coincides with the catalyst deactivation due to overoxidation. The lower initial catalyst potential compared with the carbon-supported catalyst indicates the lower initial acid formation rate. However, the magnitude of the measured potentials for the oxidised state appears to be lower, but in view of the limitation of the measurement technique, this is not considered to be significant [54].

Fig. 5a shows that the developed model, with the rate constants as given in Table 7, is well able to describe the observed reaction rates under different pH conditions. The increase in the reaction rate with increasing pH is followed by an 80% decrease for pH 9, during a reaction period of 5000 s, due to strong catalyst deactivation caused by overoxidation. The calculated potentials presented in Fig. 5b show the right magnitude for the increase in the reaction rate with increasing potential from the reduced state followed by catalyst deactivation with increasing pH corresponding to an oxidised potential level of approximately 1 V. The catalyst deactivation due to overoxidation can be seen through the simulated oxide coverage against time in Fig. 5c. After 5000 s, at pH 6, approximately 60% ($\Theta_{ox} = 0.62$) of

the catalyst surface is covered with inactive platinum oxide whereas at pH 9, approximately 80% ($\Theta_{ox} = 0.72$) of the catalyst surface is covered with inactive platinum oxide. This means with increasing pH from 6 to 9, the rate of deactivation due to overoxidation increases by 20%, higher than the rate observed for the carbon-supported catalyst.

Fig. 5d shows the simulated concentration of the intermediate aldehyde, methyl α-D-aldehydoglucopyranoside, against time. It can be seen that the selectivity for the aldehyde decreases with increasing pH, as observed for the carbon-supported catalyst. However, the maximum concentration of aldehyde (4.5 mol m^{-3}) is observed to be almost 4.5 times higher than for the carbon-supported catalyst, at pH 6. This can be seen through the lower apparent aldehyde disappearance parameter ($k_5 + k_6 C_{OH}$) for the graphite-supported catalyst compared with the carbon-supported catalyst, at pH 6. The possible explanation for this, although intrinsic conditions are considered for organic compounds, can be that the rate of the intermediate aldehyde disappearance is relatively high and hence pore diffusion limitations might be present for the aldehyde transfer, especially in the case of the carbon-supported catalyst, which has higher active metal dispersion compared with the graphite-supported catalyst.

Fig. 5e shows the simulated oxygen coverage with time. It can be seen that the initial oxygen coverage decreases with increasing pH, and a maximum coverage of around 0.4 is observed at pH 6, compared with the coverage of 0.6 for the platinum-on-carbon catalyst. This is the result of a higher oxygen reduction rate for the graphite-supported catalyst. Fig. 5f shows the simulated concentration of the reactant alcohol, MGP, as a function of time. It can be seen that the calculated conversion, from MGP concentration data, is around 18–20% over a reaction time of 5000 s. Within this conversion level, it can be accepted that the MGP oxidation displays close to 100% selectivity.

6. Conclusions

In the present work, a dynamic electrochemical kinetic model has been developed that describes the observed pH effect and catalyst deactivation due to overoxidation. The rate-determining steps and the model parameters have been deduced from previous reaction rate measurements in a CSTR, with graphite-supported Pt catalyst [28], and from stirred slurry semi-batch reaction rate data, with carbon- and graphite-supported Pt catalyst (this work). The effect of pH is incorporated by the consideration of parallel reaction steps depending on the acidity or the alkalinity of the medium. Hydroxyl ions are mainly responsible for strong deactivation of the catalyst in alkaline medium, whereas in neutral or acidic medium the deactivation is due to strong adsorption of oxygen atoms only. In both cases, the formation of inactive platinum oxide is responsible for the catalyst deactivation. The two types of catalyst show the same degree of vulnerability to deactivation due to overoxidation. However, the carbon-supported Pt catalyst gives higher initial reaction rates compared with the graphite-supported catalyst. The modelling results confirm that the intermediate aldehyde is present at low pH and the selectivity towards the aldehyde decreases with increasing pH. The graphite-supported Pt catalyst gives an intermediate aldehyde concentration almost four times higher than that obtained with the carbon-supported catalyst. However, pore diffusion limitation can result in estimates of the rate parameters of a highly reactive intermediate that are too low. The observed catalyst potential gives useful information on the oxidation state of the catalyst. The developed model can describe well the observed catalyst potential at varying pH.

References

[1] A.F. Lee, J.J. Gee, H.J. Theyers, Green Chem. 2 (2000) 279–282.
[2] T. Mallat, A. Baiker, Chem. Reviews 104 (2004) 3037–3958.
[3] H. van Bekkum, in: F.W. Lichtenthaler (Ed.), Carbohydrate as Organic Raw Materials, Wiley–VCH, Weinheim, 1990, p. 289.
[4] T. Mallat, A. Baiker, Catal. Today 19 (1994) 247–284.
[5] M. Besson, P. Gallezot, Catal. Today 57 (2000) 127–141.
[6] K. Heyns, H. Paulsen, Adv. Carbohydr. Chem. 17 (1962) 169–211.
[7] H.G.J. de Wilt, H.S. van der Baan, Ind. Eng. Chem. Prod. Res. Develop. 11 (1972) 374–378.
[8] Y. Schuurman, B.F.M. Kuster, K. van der Wiele, G.B. Marin, Appl. Catal. A 25 (1992) 31–46.
[9] Y. Önal, S. Schimpf, P. Claus, J. Catal. 223 (2004) 122–133.
[10] J.M.H. Dirkx, H.S. van der Baan, J. Catal. 67 (1981) 14–20.
[11] J.H. Vleeming, B.F.M. Kuster, G.B. Marin, Carbohydr. Res. 303 (1997) 175–183.
[12] A. Abbadi, H. van Bekkum, J. Mol. Catal. A 97 (1995) 111–118.
[13] P. Vinke, W. van der Poel, H. van Bekkum, Stud. Surf. Sci. Catal. 71 (1991) 385–394.
[14] T. Mallat, A. Baiker, L. Botz, Appl. Catal. A 86 (1992) 147–163.
[15] R. DiCosimo, G.M. Whitesides, J. Phys. Chem. 93 (1989) 768–775.
[16] J.A.A. van den Tillaart, B.F.M. Kuster, G.B. Marin, Appl. Catal. A 120 (1994) 127–145.
[17] J.H.J. Kluytmans, A.P. Markusse, B.F.M. Kuster, G.B. Marin, J.C. Schouten, Catal. Today 57 (2000) 143–155.
[18] R. Parsons, T. VanderNoot, J. Electroanal. Chem. 23 (1–2) (1988) 9–45.
[19] I.T. Bae, X. Xing, C.C. Liu, E. Yeager, J. Electroanal. Chem. 284 (1990) 335–349.
[20] B. Beden, J.M. Leger, C. Lamy, in: J.O'M. Bockris, B.E. Conway, R.E. White (Eds.), Modern Aspects of Electrochemistry, vol. 22, Elsevier, Amsterdam, 1992, p. 97.
[21] A.V. Tripkovic, K.D. Popovic, B.N. Grgur, B. Blizanac, P.N. Ross, N.M. Markovic, Electrochim. Acta 47 (2002) 3707–3714.
[22] S. Motoo, M. Watanabe, J. Electroanal. Chem. 98 (1979) 203–211.
[23] M. Mavrikakis, M.A. Barteau, J. Mol. Catal. A 131 (1998) 135–147.
[24] J.L. Davis, M.A. Barteau, Surf. Sci. 268 (1992) 11–24.
[25] C. Keresszegi, T. Brgi, T. Mallat, A. Baiker, J. Catal. 211 (2002) 244–251.
[26] P.J.M. Dijkgraaf, M.J.M. Rijk, J. Meuldijk, K. van der Wiele, J. Catal. 112 (1988) 329–336.
[27] M. Besson, F. Lahmer, P. Gallezot, G. Fleche, P. Fuertes, J. Catal. 152 (1995) 116–121.
[28] J.H. Vleeming, B.F.M. Kuster, G.B. Marin, Ind. Eng. Chem. Res. 36 (1997) 3541–3553.
[29] M. Besson, P. Gallezot, Catal. Today 81 (2004) 547–559.

[30] J.F.E. Gootzen, A.H. Wonders, A.P. Cox, W. Visscher, J.A.R. van Veen, J. Mol. Catal. A 127 (1997) 113–131.
[31] A.P. Markusse, B.F.M. Kuster, J.C. Schouten, Catal. Today 66 (2001) 191–197.
[32] V.R. Gangwal, B.G.M. van Wachem, B.F.M. Kuster, J.C. Schouten, Chem. Eng. Sci. 57 (2002) 5051–5063.
[33] V.R. Gangwal, J. van der Schaaf, B.F.M. Kuster, J.C. Schouten, Catal. Today 96 (2004) 223–234.
[34] E. Muller, K. Schwabe, Z. Electrochim. Acta 33 (1928) 170.
[35] M. Rottenberg, Baertschi, Helv. Chim. Acta 227 (1956) 1073.
[36] G. de Wit, J.J. de Vlieger, A.C. Kock-van Dalen, R.H. Rob Laroy, A.J. van Hengstum, A.P.G. Kieboom, H. van Bekkum, Carbohydr. Res. 91 (1981) 125–138.
[37] T. Mallat, Z. Bodnar, A. Baiker, O. Greis, H. Strubig, A. Reller, J. Catal. 142 (1993) 237–253.
[38] T. Mallat, Z. Bodnar, P. Hug, A. Baiker, J. Catal. 153 (1995) 131–143.
[39] P. Gallezot, Catal. Today 37 (1997) 405–418.
[40] T. Engel, G. Ertl, in: D.A. King, D.P. Woodruff (Eds.), Chemical Physics of Solid Surfaces and Heterogeneous Catalysis, vol. 4, Elsevier, Amsterdam, 1982, p. 73.
[41] R. Thacker, J.P. Hoare, J. Electroanal. Chem. 30 (1971) 1–14.
[42] J.L. Gland, B.A. Sexton, G.B. Fisher, Surf. Sci. 95 (2–3) (1980) 587–602.
[43] G. Horanyi, Catal. Today 19 (1994) 285–312.
[44] H. Wroblowa, M.L.B. Rao, A. Damjanovic, J.O'M. Bockris, J. Electroanal. Chem. 15 (1967) 139–150.
[45] C. Harting, M.T.M. Koper, J. Electroanal. Chem. 532 (2002) 165–170.
[46] P. Vinke, D. de Wilt, A.T.J.W. de Goede, H. van Bekkum, Stud. Surf. Sci. Catal. 72 (1992) 1.
[47] L. Jelemensky, B.F.M. Kuster, G.B. Marin, Chem. Eng. Sci. 51 (10) (1996) 1767–1776.
[48] V.R. Gangwal, J. van der Schaaf, B.F.M. Kuster, J.C. Schouten, Appl. Catal. A 274 (2004) 275–283.
[49] A. Constantinides, N. Mostoufi, Numerical Methods for Chemical Engineers with MATLAB Applications, Prentice Hall Inc., Englewood Cliffs, 1999.
[50] P. Briot, A. Auroux, D. Jones, M. Primet, Appl. Catal. 59 (1990) 141–152.
[51] M.L. Sattler, P.N. Ross, Ultramicroscopy 20 (1986) 21–28.
[52] M. Peukert, T. Yoneda, R.A. Dalla Betta, M. Boudart, J. Electrochem. Soc. 5 (1986) 944–947.
[53] J.M.H. Dirkx, The oxidation of carbohydrates with platinum on carbon as catalyst, Ph.D. thesis, Eindhoven University of Technology, Eindhoven, The Netherlands, 1977.
[54] T. Mallat, A. Baiker, Top. Catal. 8 (1999) 115–124.